

SCIENTIFIC REPORTS

OPEN

THz Electric Field-Induced Second Harmonic Generation in Inorganic Ferroelectric

Kirill A. Grishunin¹, Nikita A. Ilyin¹, Natalia E. Sherstyuk¹, Elena D. Mishina¹, Alexey Kimel^{1,2}, Vladimir M. Mukhortov³, Andrey V. Ovchinnikov⁴, Oleg V. Chefonov⁴ & Mikhail B. Agranat⁴

Second Harmonic Generation induced by the electric field of a strong nearly single-cycle terahertz pulse with the peak amplitude of 300 kV/cm is studied in a classical inorganic ferroelectric thin film of $(\text{Ba}_{0.8}\text{Sr}_{0.2})\text{TiO}_3$. The dependences of the SHG intensity on the polarization of the incoming light is revealed and interpreted in terms of electric polarization induced in the plane of the film. As the THz pulse pumps the medium in the range of phononic excitations, the induced polarization is explained as a dynamical change of the ferroelectric order parameter. It is estimated that under action of the THz pulse the ferroelectric order parameter acquires an in-plane component up to 6% of the net polarization.

Photoinduced nonequilibrium phase transitions triggered by femtosecond or picosecond laser pulses is a subject of intense and multidisciplinary research^{1,2}. Fundamentally, these are counterintuitive phenomena in which subtle excitations of atoms or spins are able to lead to dramatic changes in crystallographic, electric, or magnetic properties of media. In ferroics, ultrafast control of the order parameter (electric polarization or magnetization) is a particularly important problem, understanding of which might be essential for future progress in information processing technology. In the last decades a substantial progress has been achieved in ultrafast optical control of spins in magnetically ordered materials and all-optical magnetic recording. It has been shown that exciting magnets on a timescale much faster than characteristic times of atomic, orbital and spin motion can steer magnetization dynamics along yet unexplored non-thermodynamic routes³. Ultrafast coherent control of the magnetic phase transitions via active optical pumping of the soft mode^{4,5} and magnetization reversal via a strongly non-equilibrium state⁶ have been demonstrated. Thermodynamically, critical behaviors of the electric polarization and the magnetization are very similar⁷. Nevertheless, the possibility of switching of the electric polarization by ultrashort laser pulses has not been reported until now. Naturally it raises interests to the problem of ultrafast optical control of electric polarization in ferroelectric materials.

Despite the enormous amount of experiments reporting on optical control of spins, there are very few studies of ultrafast dynamics of the electric polarization^{8–16}. Obviously, measurement techniques based on electric contacts are not able to provide the required temporal resolution. An elegant solution for a detection of the order parameter in ferroelectrics can be based on time-resolved X-ray diffraction. However, this technique is very challenging and, as a matter of fact, it is available in very few places in the world^{17–19}. Nonlinear optical technique of the Second Harmonic Generation (SHG) is known to be very sensitive to the order parameter in ferroelectrics^{16, 20–22} and it is by far less challenging than the studies in the X-ray spectral range^{23–25}. However, despite this fact practically nothing is known about ultrafast nonlinear optical response of ferroelectrics²⁶. Consequently, this lack of knowledge considerably hampers optimization and interpretation of experiments in which ultrafast dynamics in ferroics is probed with the help of second harmonic generation and visible light.

Here we report about experimental study of ultrafast nonlinear optical response of ferroelectric $(\text{Ba}_{0.8}\text{Sr}_{0.2})\text{TiO}_3$ (BST) to the electric field of nearly single-cycle THz pulses picosecond pulses. For this we employ a pump-probe method. Freely propagating nearly single-cycle THz pulses with the amplitude up to 300 kV/cm excites ferroelectric $(\text{Ba}_{0.8}\text{Sr}_{0.2})\text{TiO}_3$ film. Femtosecond pulses in the near-infrared spectral range probe the response of the system by SHG. Analysis of the time-resolved non-linear optical response reveals that the

¹Moscow Technological University, MIREA, Vernadsky Ave. 78, 119454, Moscow, Russia. ²Institute for Molecules and Materials, Radboud University Nijmegen, 6525, AJ, Nijmegen, The Netherlands. ³Southern Scientific Center of Russian Academy of Sciences, Chehova 41, Rostov-on-Don, 344006, Russia. ⁴Joint Institute for High Temperatures of Russian Academy of Sciences (JIHT), Izhorskaya st. 13 Bd. 2, 125412, Moscow, Russia. Correspondence and requests for materials should be addressed to K.A.G. (email: grishunin@mirea.ru)

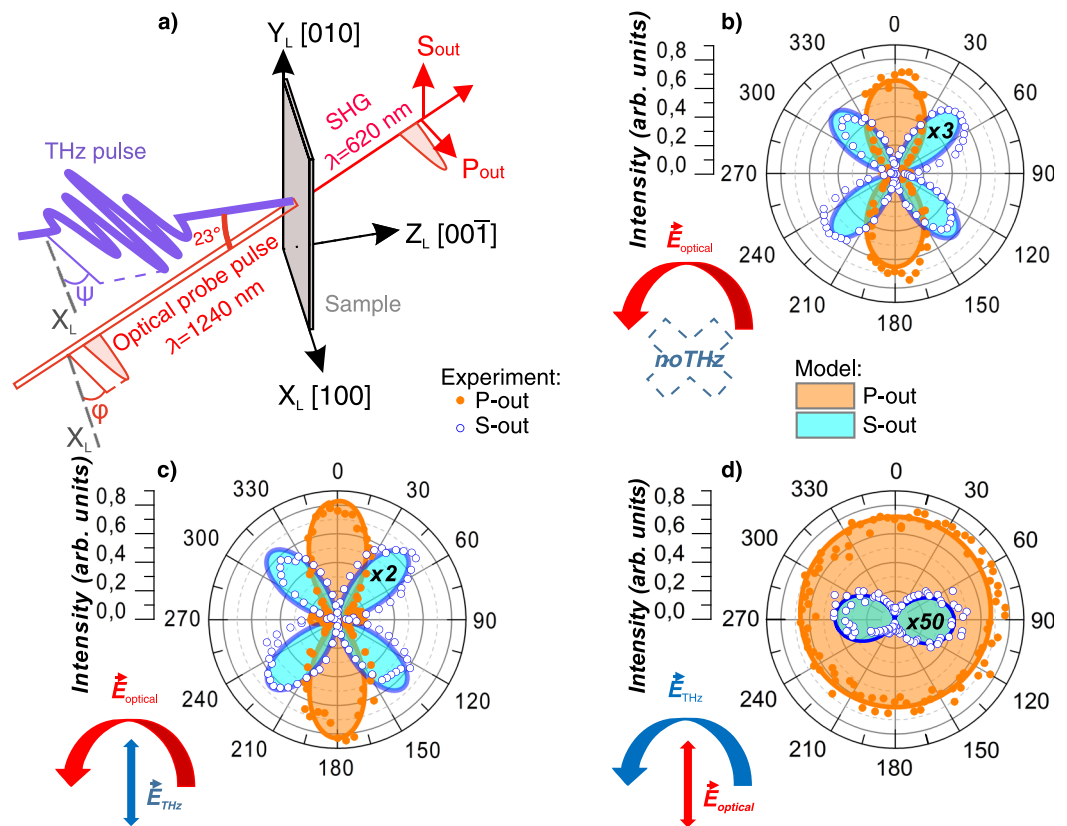


Figure 1. Experimental geometry and polarization diagrams of the SHG intensity for various experimental geometries. **(a)** Experimental geometry. The axes of the chosen laboratory frame X_L , Y_L , Z_L correspond to $[100]$, $[010]$ and $[00\bar{1}]$ crystallographic directions, respectively. φ - the angle between the electric field of near-infrared probe and the X_L -axis; ψ - the angle between the electric field of the THz pump pulse and the X_L -axis; **(b)** dependence of the SHG signal on φ without any THz pump; **(c)** dependence of the SHG signal on φ when the THz field is applied parallel with respect to the X_L -axis. The polarization of the SHG signal was set either in the P_{out} or S_{out} -state; **(d)** dependence of the SHG signal on ψ when the probe polarization was set to the P-state ($\varphi=0$). The polarization of the SHG signal was set either in the P_{out} or S_{out} -state. Dots correspond to experimental data and lines are fits (calculations see in Supplementary Information). Values for S-state multiplied by 3, 2 and 50 for **(b–d)** respectively.

experimental results can be explained assuming that under action of the THz pulse the ferroelectric order parameter acquires an in-plane component up to 6% of the net polarization.

Results

We have used single-cycle THz pulses to excite the ferroelectric. The result of the excitation was probed by a femtosecond laser with the central wavelength of 1240 nm. Upon non-linear interaction of this pulse with the ferroelectric medium, second harmonic light was generated with the central wavelength of 620 nm. The time delay τ_d between the THz-pump and optical-probe pulses was changed with the help of a delay line. The pump beam was at normal incidence. The angle of incidence of the probe beam was 23 degrees. Schematics of the experimental setup is shown in Fig. 1a. In the following orientation of the electric fields of the pump and probe pulses will be described in laboratory frame with X_L , Y_L and Z_L axes, as shown in the figure. The sample was oriented with its $[100]$ axis parallel to the X_L axis. The electric field vector of the THz pump pulse was oriented in the $X_L Y_L$ plane at angle ψ with respect to the X_L axis. The electric field (i.e. polarization) of the near-infrared probe pulse could be rotated with respect to the X_L axis by angle φ or set in the P-state ($\varphi=0$). The polarization of the second harmonic light was chosen either in the P- or S-states of incidence (P_{out} or S_{out} in Fig. 1a, respectively).

In the first experiment, time-delay between pump and probe pulses τ_d was set to zero. The detected SHG signal of the P_{out} and S_{out} polarizations was studied as a function of the probe polarization angle φ . With no THz electric field, the SHG intensities reveal two-fold and four-fold polarization dependencies (see Fig. 1b). If the strong THz field is applied to the ferroelectric material and $\psi=0$, the intensity of the SHG signal slightly increases, but the polarization dependences remain qualitatively the same (Fig. 1c).

In the second experiment, we fixed the polarization of the near-infrared probe pulse in the P-state and rotated the electric field of the THz pulse changing ψ . If the polarization of the outgoing second harmonic light is in the P_{out} -state, the SHG intensity only slightly depends on ψ . For the S_{out} -state of the SHG signal, the dependence is twofold with the maxima when the THz field is along the X_L axis ($\psi=0$).

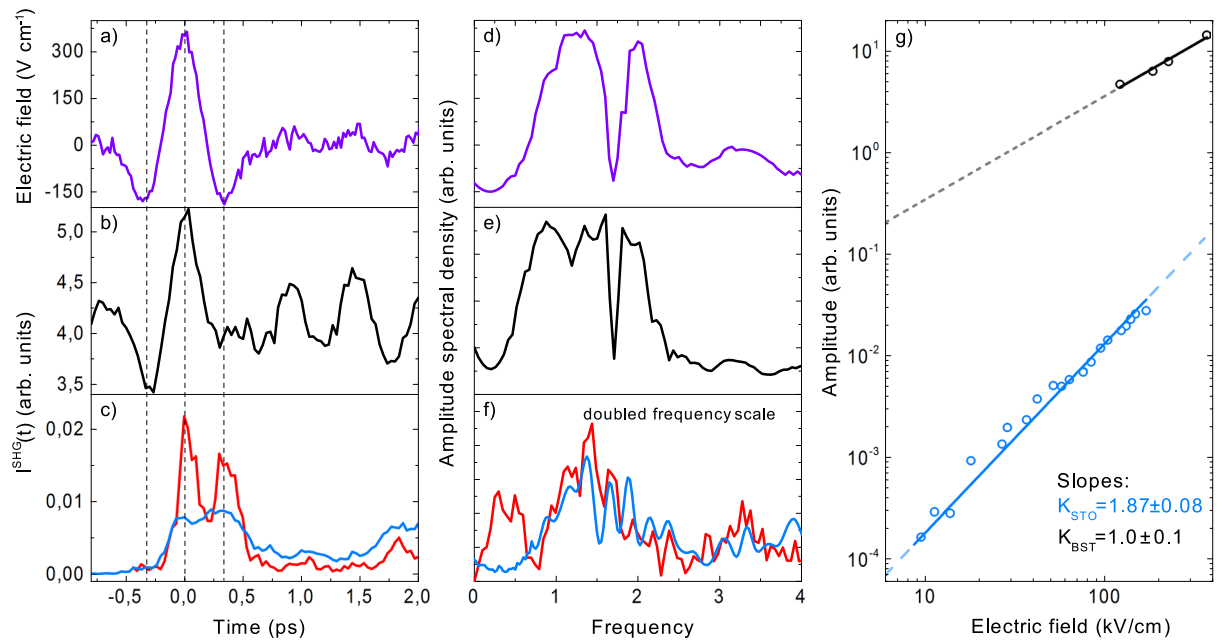


Figure 2. THz-induced dynamics of nonlinear-optical response of the crystals. **(a)** Time trace of the electric field of the THz pump pulse; intensities of the SHG-signal: **(b)** for BST, **(c)** for STO (red line) and Si (black line); **(d–f)** Fourier transform spectra of the time traces shown in panels **(a–c)**, respectively (**(f)** plotted in doubled frequency scale); **(g)** dependence of the SHG intensity on the THz field (logarithmic scale) for BST (top line) and STO (bottom line).

Hence the data show that the THz electric field clearly affects the process of the second harmonic generation. To reveal ultrafast dynamics of these electric field induced changes, we performed pump-probe measurements of the SHG signal. In particular, the signal was measured as a function of the delay τ_d between the THz-pump and near-infrared probe pulses. Figure 2a shows time-domain trace of the electric field of the THz pulse obtained with the help of electro-optical sampling. The measurements of the SHG signal from the BST film (Fig. 2b) reveal a similar dynamics during the overlap of the probe and THz-pump pulses. It points out that the non-linear response is proportional to the THz electric field.

For comparison, we also measured temporal evolution of the SHG signals from centrosymmetric crystals excited by the intense THz pulse. The SHG transients for SrTiO₃ (STO) and Si are shown in Fig. 2c (red and blue line, respectively). First of all, for the both cases of the centrosymmetric crystals the SHG signal of the unperturbed media are zero. Secondly, in the maximum of THz modulated signal the absolute values of the intensity of the SHG from BST is two orders of magnitude higher than those for the centrosymmetric crystals. Thirdly, the shape of the SHG response differs from the shape of the THz pulse. Qualitatively, the frequency of the time transients of the SHG response for centrosymmetric STO and Si is doubled with respect to the frequency of the temporal variations of the electric field of the THz pulse.

The spectra obtained as Fourier transforms of the time-traces for BST and STO as well as for THz pulse are plotted in Fig. 2d and e. For BST, the frequency-domain signal follows the input pulse, while for STO the frequency is doubled. Power dependencies of the SHG intensity on the THz electric field are plotted in Fig. 2f in logarithmic scale and reveal linear and quadratic for BST and STO, respectively.

Finally, from the measured SHG traces we deduced how the induced electric polarization changes upon a change of the electric field of the THz pulse. These dependencies were compared with the hysteresis loops measured with the help of the Soyer-Tower technique (Fig. 3a, bottom solid line). The first, i.e. static hysteresis loop, is quite typical for BST films with 20% of Strontium²⁷. We also compared the data with loops obtained by measuring the SHG signal in an electric field which varies with the frequency of 100 Hz. To deduce the loops we employed the procedure of reconstruction of the electric polarization as described previously²⁸. It is based on the dependence of SHG intensity on ferroelectric polarization:

$$I^{2\omega} = I_{bg}^{2\omega} + \alpha(P_0 + P(E_\Omega))^2, \quad (1)$$

where $I_{bg}^{2\omega}$ is the incoherent component of the unswitchable part of the second harmonic signal; $P(E_\Omega)$ is the ferroelectric (switchable) polarization, which depends on the electric field of the THz pulse; P_0 is remanent polarization i.e. unswitchable polarization; α is the proportionality coefficient, which is determined by the Fresnel factors and the nonlinear optical susceptibility.

In order to deduce the field dependence of the electric polarization $P(E_\Omega)$, one has to subtract from the SHG intensity the background signal $I_{bg}^{2\omega}$ which is independent on the electric field. Then one has to take the square root

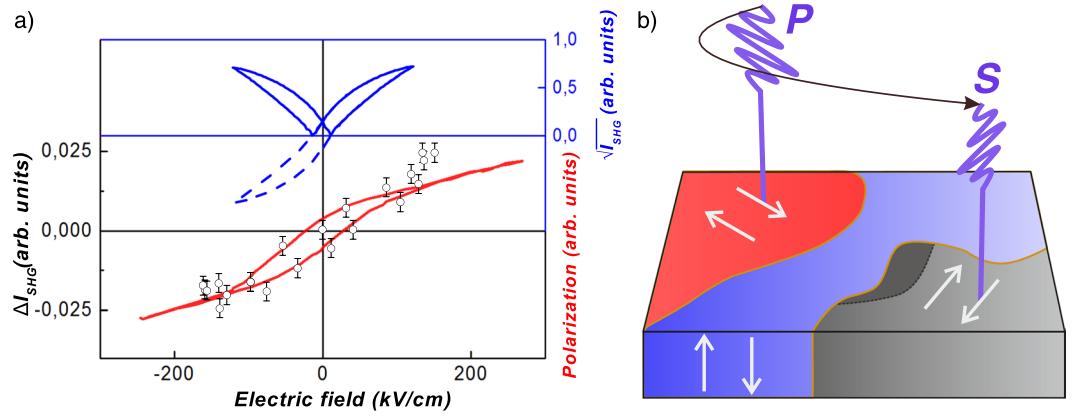


Figure 3. Effect of the electric field on electric polarization and SHG. **(a)** Hysteresis loops of the electric polarization obtained by the Soyer-Tower technique (bottom solid line); SHG hysteresis loop reconstructed from low-frequency measurements (top line). To compare with the hysteresis loop for the electric polarization, left side of the graph is plotted with an inversed sign (dashed line); SHG loops reconstructed from the experiment with THz pump pulses (points). Error bars on ΔI_{SHG} show s.d. from the 15 measured samples; **(b)** diagram showing the domain structure and its sensitivity to the external THz pulse.

from the residual signal. It gives the value, which is proportional to the electric polarization $P_0 + P(E_\Omega)$. The result of such a data processing is shown in Fig. 3a (top solid line). Additionally, we can mirror the loop with respect to the x-axis at negative electric fields and thus obtain a loop that resembles largely the dielectric hysteresis loop obtained in statics (Fig. 3a, dashed line). Since in the THz measurements both electric field and SHG intensity are measured as a function of time, hysteresis loop is set parametrically. After excluding time from these dependences and performing the same procedure for the SHG intensity (except taking the square root because of linear dependence of the SHG intensity), the THz SHG loop is obtained. In Fig. 3a points show hysteresis loops for two values of the THz electric field (E-field). Although these loops are quite noisy, a similarity with the low-frequency loop (with hysteresis and coercivity) is obvious.

Discussion

In centrosymmetric crystals (SrTiO₃, Si), in the electric-dipole approximation, it is possible to generate second harmonic signal by applying an external electric field, which breaks the inversion symmetry. This is so-called electric field induced second harmonic (EFISH). For electric field oscillating at THz frequency we will call it TEFISH. Taking into account that $\Omega \ll \omega$ and $\Omega + \omega + \omega \cong 2\omega$, TEFISH polarization can be described as $\vec{P}^{\text{TEFISH}}(2\omega) = \hat{\chi}^{(3)} \vec{E}_\Omega \vec{E}_\omega \vec{E}_\omega$. Analogously to the linear optical Kerr effect, which is described by a tensor of the same rank, it has electronic and ionic contributions²⁹.

In noncentrosymmetric crystals with nonzero electric dipole contribution $\vec{P}^{\text{cryst}}(2\omega)$, formally the same electric field induced mechanism is also valid:

$$\vec{P}(2\omega) = \vec{P}^{\text{cryst}}(2\omega) + \vec{P}^{\text{TEFISH}}(2\omega) = \hat{\chi}^{(2)} \vec{E}_\Omega \vec{E}_\omega + \hat{\chi}^{(3)} \vec{E}_\Omega \vec{E}_\omega \vec{E}_\omega. \quad (2)$$

For ferroelectric material electric field dependent nonlinear optical polarization has several contributions (analogously to linear optics²⁹⁻³¹): electronic, ionic and piezoelectric. As the employed THz pulses pump the medium in the range of phononic excitations, it is natural to assume that the THz electric field induces ferroelectric polarization due to the ionic contribution.

Without any electric field, the sample is split into two types of domains with the polarization aligned along the [001] axis. For nonzero angle of incidence, for the SHG intensity one finds $I_{2\omega} \sim (P_{2\omega}^{001})^2$.

When the in-plane electric field is applied at angle ψ respect to X_L axis, a part of the domains line up along the field. In analogy with ref. 32, the net response will be defined by volume fractions of domains V_i^+ and V_i^- ($i = x, y$) ($i = x, y$), where x, y denote the crystallographic axis along which the polarization is aligned, but “+” and “-” show the direction of the alignment. The differences of the fractions of the positively and the negatively oriented domains determines the electric field dependent contribution to the nonlinear optical polarization as $P_i = P_i^{001} + \Delta V_i P_i$, where $\Delta V_i = V_i^+ - V_i^-$.

Thus, the volume contributions to the corresponding domain directions for any angle ψ of the applied THz E-field results in the following dependences:

$$\Delta V_x = \gamma \cos \psi, \quad (3)$$

$$\Delta V_y = \gamma \sin \psi, \quad (4)$$

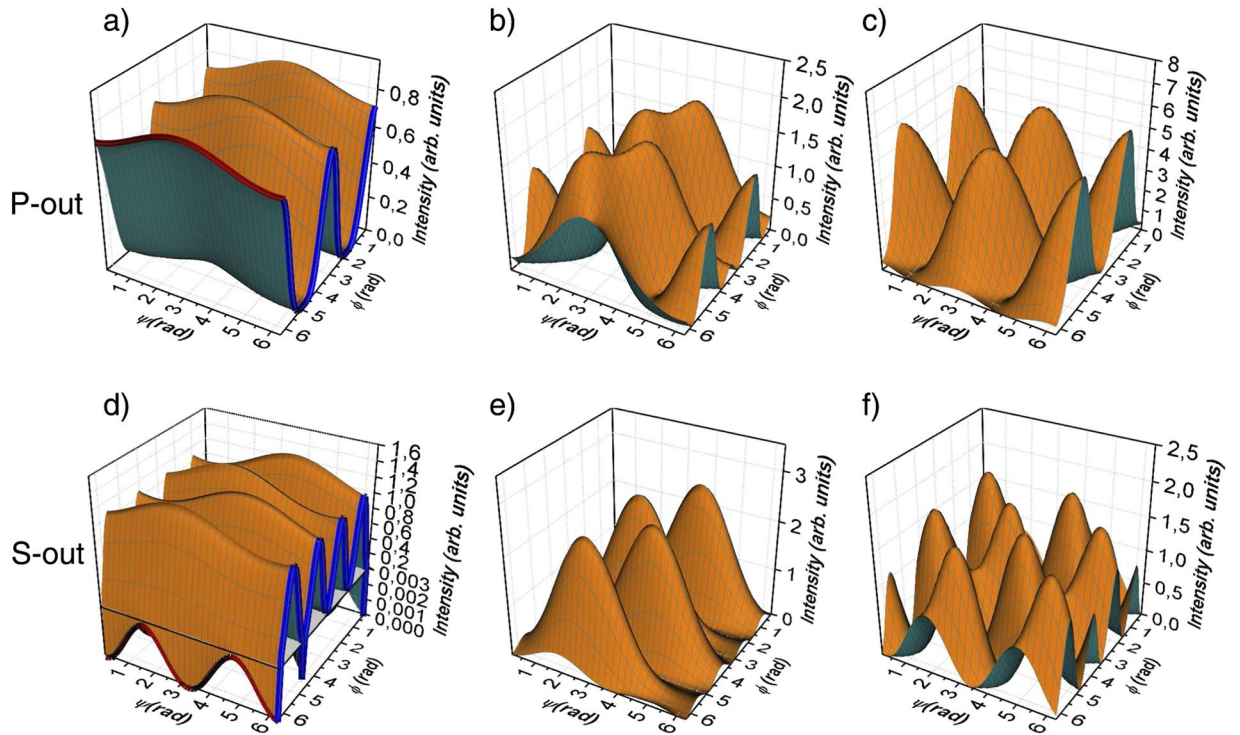


Figure 4. Polarization dependences obtained within the suggested model for different γ : **(a,d)** $\gamma = 0.05$; **(b,e)** $\gamma = 0.5$; **(c,f)** $\gamma = 1$. Blue and red lines on **(a and d)** represent the linear plots of fitting curve from Fig. 1c and d.

$$\Delta V_z = \sqrt{1 - \Delta V_x^2 - \Delta V_y^2}, \quad (5)$$

where γ is the ratio of the fraction of in-plane switched domains to the fraction of [001]-oriented unswitched domains.

Generally, SHG intensity for the THz E-field oriented along arbitrary direction in the plane of the sample can be written as

$$I_{2\omega} \propto (P_{2\omega}^{001}\Delta V_z + P_{2\omega}^{100}(E_\Omega)\Delta V_x + P_{2\omega}^{010}(E_\Omega)\Delta V_y)^2. \quad (6)$$

When the in-plane electric field is applied along the [100] axis ($V_x \neq 0, V_y = 0$), a polarization is induced along the same axis and the intensity acquires an additional contribution:

$$I_{2\omega} \propto (P_{2\omega}^{001}\Delta V_z)^2 + 2P_{2\omega}^{001}P_{2\omega}^{100}(E_\Omega)\Delta V_z\Delta V_x + (P_{2\omega}^{100}(E_\Omega)\Delta V_x)^2. \quad (7)$$

Analogously, similar dependences of the SHG intensity can be written for the case of THz field, oriented along the y axis. Such a field promotes formation of ΔV_y domains.

The results based on the suggested model show a good agreement with the experimental data (Fig. 1). In the simultaneous fit only 2 meaningful and 1 calibration fitting parameters were used giving $\chi_1/\chi_2 = 3.4 \pm 0.3$ for the wavelength of the probing light of 1240 nm (compare $\chi_1/\chi_2 = 2.6 \pm 0.4$ for the wavelength of 1058 nm³³ for BaTiO₃) and $\gamma = 0.06$ (calculations for the cases represented on Fig. 1 see in Supplementary Information).

Figure 4 shows examples of polarization dependences obtained for different γ . An increase of γ results in an increase of the SHG intensity and changes in polarization dependences. When the THz electric field is rotated, asymmetry of one-fold $I_{2\omega}(\psi)$ first increases (Fig. 4b and e), but then for $\gamma \rightarrow 1$ the dependences acquire a two-fold symmetry. When optical polarization is rotated, four-fold $I_{2\omega}(\varphi)$ dependence for the S_{out} state of the SHG electric field changes only in intensity. For the P_{out} state, the two-fold $I_{2\omega}(\varphi)$ dependence changes passing through four-fold dependence. Cross-sections of the 3D plots along the planes (blue and red lines on Fig. 4a and d) represent the linear plots of the fitting curve from Fig. 1c and d, respectively.

The question arises: can we really switch out-of-plane domains by an in-plane electric field? Very recently it was shown that in classical ferroelectric Pb(Zr_{0.4}Ti_{0.6})O₃ domain nucleation time under electric field of 200 kV/cm was about 0.47 ps³⁴. The strength of the electric field required for the switching and nucleation time are very close to the amplitude and the period of the THz electric field used in our experiments. Thus, it seems that in our experiment a switching of the 90-degree ferroelectric domains, as schematically shown in Fig. 3b, may indeed take place.

Conclusions

In our experiments with ferroelectric thin film, we observed a very strong modulation of the SHG signal by the electric field of a THz nearly single cycle pulse. Polarization dependences of the SHG intensity were explained in terms of THz electric field-induced second harmonics generation THz EFISH. As the THz pulse pumps the medium in the range of phononic excitations, the modulation of the nonlinear signal can be explained in terms of a change of the ferroelectric order parameter. In particular, under action of the THz pulse the latter acquires an in-plane component up to 6% of the net polarization.

The net SHG signal responds to the THz excitation as if the THz pulse induces a 90-degree switching of the polarization in parts of the sample. The possibility of such a switching on the time scale of the period of the soft mode was recently suggested by ref. 34.

Methods

Samples. Heteroepitaxial $(\text{Ba}_{0.8}\text{Sr}_{0.2})\text{TiO}_3$ (BST) thin film (thickness 500 nm) was deposited on MgO (001) substrate by RF-sputtering of stoichiometric polycrystalline target. Transparent and mirror-smooth film was realized by means of layer-by-layer growth (Frank-van der Merwe mechanism). Details of the growth conditions have been previously reported in ref. 35. The vertical and azimuthal film misorientations were found to be less than 0.4° by high resolution XRD analysis. $(\text{Ba}_{0.8}\text{Sr}_{0.2})\text{TiO}_3$ solid solutions belong to ferroelectric perovskites. In the paraelectric phase, they have a cubic unit cell (space group Pm3m). In the ferroelectric phase below the Curie temperature ($T_c = 353$ K) they have a tetragonal unit cell (space group P4mm, point group 4mm). At room temperature, the soft mode is overdamped with the following parameters: $\Omega = 46 \text{ cm}^{-1}$ (2.40 THz), $\Delta\Omega = 50 \text{ cm}^{-1}$ (1.5 THz)^{36,37}. The as-grown film consists of 180-degree domains which are not compensated due to an interfacial strain and show built-in polarization in the [001] crystallographic direction^{37,38}. The size of domains is about 500 nm.

Experimental setup. The THz pulses were generated by optical rectification of the femtosecond laser pulses, generated by high-energy 10 Hz Cr:Forsterite chirped-pulse amplification laser at the central wavelength of 1240 nm with 100 fs pulse duration and 20 mJ output energy, in the nonlinear organic crystal OH1³⁹. The polarization of the terahertz pulse coincided with the polarization of the femtosecond pump laser pulse. The rotation of the terahertz electric field was carried out by simultaneous rotation of polarization of incident beam and nonlinear organic crystal OH1 on the same angle. The energy of the THz pulses was up to $2 \mu\text{J}$ at pump laser energy of $700 \mu\text{J}$. Two parabolic mirrors were used to guide and to focus the THz pulses on the sample surface. The first mirror collected and collimated THz pulses emitted from the nonlinear crystal. The second one focused the THz beam into a spot with the diameter of $900 \mu\text{m}$. Such parameters provided a high amplitude of the THz electric field up to 300 kV/cm . The amplitude of the THz electric field was estimated based on the measurements of the pulse duration and pulse fluence. We have used about 3% of the output energy of the Cr:Forsterite laser beam reflected by a thin optical glass plate to probe the electric polarization in the studied medium. These optical probe pulses passed through a delay line and were focused into a spot of $200 \mu\text{m}$ in diameter. After the sample, the fundamental optical radiation at the wavelength of 1240 nm was blocked and the SHG signal at the wavelength of 620 nm was transmitted by a bandpass filter ($\Delta\lambda = 10 \text{ nm}$). The SHG signal was detected by a Photo-Multiplier Tube in the current regime.

References

- Nagaya, K. *et al.* Ultrafast Dynamics of a Nucleobase Analogue Illuminated by a Short Intense X-ray Free Electron Laser Pulse. *Physical Review X* **6**, 021035, doi:10.1103/PhysRevX.6.021035 (2016).
- Canton, S. E. *et al.* Visualizing the non-equilibrium dynamics of photoinduced intramolecular electron transfer with femtosecond X-ray pulses. *Nature Communications* **6**, 6359, doi:10.1038/ncomms7359 (2015).
- Bossini, D., Belotelov, V. I., Zvezdin, A. K., Kalish, A. N. & Kimel, A. V. Magnetoplasmonics and Femtosecond Optomagnetism at the Nanoscale. *ACS Photonics* **3**, 1385–1400, doi:10.1021/acsphotonics.6b00107 (2016).
- De Jong, J. A. *et al.* Coherent control of the route of an ultrafast magnetic phase transition via low-amplitude spin precession. *Physical Review Letters* **108**, 157601, doi:10.1103/PhysRevLett.108.157601 (2012).
- Afanasiev, D. *et al.* Control of the Ultrafast Photoinduced Magnetization across the Morin Transition in DyFeO_3 . *Physical Review Letters* **116**, 097401, doi:10.1103/PhysRevLett.116.097401 (2016).
- Vahaplar, K. *et al.* Ultrafast Path for Optical Magnetization Reversal via a Strongly Nonequilibrium State. *Physical Review Letters* **103**, doi:10.1103/PhysRevLett.103.117201 (2009).
- Landau, L. & Lifshitz, E. *Electrodynamics of continuous media* (Pergamon, Oxford, 1984).
- Rana, D. S. *et al.* Understanding the nature of ultrafast polarization dynamics of ferroelectric memory in the multiferroic BiFeO_3 . *Advanced Materials* **21**, 2881–2885, doi:10.1002/adma.200802094 (2009).
- Bhattacharjee, S., Rahmedov, D., Wang, D., Íñiguez, J. & Bellaiche, L. Ultrafast switching of the electric polarization and magnetic chirality in BiFeO_3 by an electric field. *Physical Review Letters* **112**, doi:10.1103/PhysRevLett.112.147601 (2014).
- Brekhov, K. A. *et al.* Photoinduced dynamics and femtosecond excitation of phonon modes in ferroelectric semiconductor $\text{Sn}_2\text{P}_2\text{S}_6$. *JETP Letters* **102**, 372–377, doi:10.1134/S0021364015180034 (2015).
- Miyamoto, T., Yada, H., Yamakawa, H. & Okamoto, H. Ultrafast modulation of polarization amplitude by terahertz fields in electronic-type organic ferroelectrics. *Nature Communications* **4**, 2586, doi:10.1038/ncomms3586 (2013).
- Yamakawa, H. *et al.* Novel electronic ferroelectricity in an organic charge-order insulator investigated with terahertz-pump optical-probe spectroscopy. *Scientific Reports* **6**, 20571, doi:10.1038/srep20571 (2016).
- Kampfrath, T., Tanaka, K. & Nelson, K. A. Resonant and nonresonant control over matter and light by intense terahertz transients. *Nature Photonics* **7**, 680–690, doi:10.1038/nphoton.2013.184 (2013).
- Katayama, I. *et al.* Ferroelectric Soft Mode in a SrTiO_3 Thin Film Impulsively Driven to the Anharmonic Regime Using Intense Picosecond Terahertz Pulses. *Physical Review Letters* **108**, 097401, doi:10.1103/PhysRevLett.108.097401 (2012).
- Qi, T., Shin, Y.-H., Yeh, K.-L., Nelson, K. A. & Rappe, A. M. Collective Coherent Control: Synchronization of Polarization in Ferroelectric PbTiO_3 by Shaped THz Fields. *Physical Review Letters* **102**, 247603, doi:10.1103/PhysRevLett.102.247603 (2009).
- Cornet, M., Degert, J., Abraham, E. & Freysz, E. Terahertz-field-induced second harmonic generation through Pockels effect in zinc telluride crystal. *Optics Letters* **39**, 5921, doi:10.1364/OL.39.005921 (2014).
- Hruszkewycz, S. O. *et al.* Imaging local polarization in ferroelectric thin films by coherent X-ray bragg projection ptychography. *Physical Review Letters* **110**, doi:10.1103/PhysRevLett.110.177601 (2013).

18. Schmising, C. V. K., Bargheer, M., Woerner, M. & Elsaesser, T. Real-time studies of reversible lattice dynamics by femtosecond X-ray diffraction. *Zeitschrift für Kristallographie* **223**, 283–291, doi:[10.1524/zkri.2008.0028](https://doi.org/10.1524/zkri.2008.0028) (2008).
19. Oguz Er, A., Chen, J. & Rentzepis, P. M. Ultrafast time resolved x-ray diffraction, extended x-ray absorption fine structure and x-ray absorption near edge structure. *Journal of Applied Physics* **112**, doi:[10.1063/1.4738372](https://doi.org/10.1063/1.4738372) (2012).
20. Jiang, A. Q., Scott, J. F., Lu, H. & Chen, Z. Phase transitions and polarizations in epitaxial BaTiO₃/SrTiO₃ superlattices studied by second-harmonic generation. *Journal of Applied Physics* **93**, 1180–1185, doi:[10.1063/1.1533094](https://doi.org/10.1063/1.1533094) (2003).
21. Sherstyuk, N. E. *et al.* Optical Second Harmonic Generation Microscopy for Ferroic Materials. *Ferroelectrics* **477**, 29–46, doi:[10.1080/000150193.2015.999597](https://doi.org/10.1080/000150193.2015.999597) (2015).
22. Grishunin, K. A., Brekhov, K. A. & O. V., S. The study of the nature of the local optical inhomogeneities induced by ultrashort laser pulses, in the crystal of the ferroelectric-semiconductor Sn₂P₂S₆. *Russian Technological Journal* **2**, 134–144 (2015).
23. Fong, D. D. & Thompson, C. *In Situ* Synchrotron X-Ray Studies of Ferroelectric Thin Films. *Annual Review of Materials Research* **36**, 431–465, doi:[10.1146/annurev.matsci.36.090804.100242](https://doi.org/10.1146/annurev.matsci.36.090804.100242) (2006).
24. Ejdrup, T. *et al.* Picosecond time-resolved laser pump/X-ray probe experiments using a gated single-photon-counting area detector. *Journal of Synchrotron Radiation* **16**, 387–390, doi:[10.1107/S0909049509004658](https://doi.org/10.1107/S0909049509004658) (2009).
25. Grübel, S. *et al.* Ultrafast x-ray diffraction of a ferroelectric soft mode driven by broadband terahertz pulses. *arXiv* 1–5, 1602.05435 (2016).
26. Chen, F. *et al.* Ultrafast Terahertz Gating of the Polarization and Giant Nonlinear Optical Response in BiFeO₃ Thin Films. *Advanced Materials* **27**, 6371–6375, doi:[10.1002/adma.201502975](https://doi.org/10.1002/adma.201502975) (2015).
27. Shirokov, V. B., Biryukov, S. V., Mukhortov, V. M. & Yuzyuk, Y. I. Polarization of thin barium-strontium titanate films by an external electric field. *Technical Physics* **56**, 1175–1180, doi:[10.1134/S106378421108024X](https://doi.org/10.1134/S106378421108024X) (2011).
28. Mishina, E., Sherstyuk, N., Golovko, Y., Muhortov, V. & Sigov, A. Polarization switching in ferroelectric thin films studied by optical second harmonic generation. *Integrated Ferroelectrics* **92**, 65–76, doi:[10.1080/10584580701746913](https://doi.org/10.1080/10584580701746913) (2007).
29. Wang, F. Calculation of the electro-optical and nonlinear optical coefficients of ferroelectric materials from their linear properties. *Physical Review B* **59**, 9733–9736, doi:[10.1103/PhysRevB.59.9733](https://doi.org/10.1103/PhysRevB.59.9733) (1999).
30. Veithen, M., Gonze, X. & Ghosez, P. First-principles study of the electro-optic effect in ferroelectric oxides. *Physical Review Letters* **93**, doi:[10.1103/PhysRevLett.93.187401](https://doi.org/10.1103/PhysRevLett.93.187401) (2004).
31. Gopalan, V. & Mitchell, T. E. *In situ* video observation of 180° domain switching in LiTaO₃ by electro-optic imaging microscopy. *Journal of Applied Physics* **85**, 2304, doi:[10.1063/1.369542](https://doi.org/10.1063/1.369542) (1999).
32. Mishina, E. D. *et al.* Domain orientation in ultrathin (Ba,Sr)TiO₃ films measured by optical second harmonic generation. *Journal of Applied Physics* **93**, 6216, doi:[10.1063/1.1563849](https://doi.org/10.1063/1.1563849) (2003).
33. Miller, R. C., Kleinman, D. A. & Savage, A. Quantitative Studies of Optical Harmonic Generation in CdS, BaTiO₃, and KH₂PO₄ Type Crystals. *Physical Review Letters* **11**, 146–149, doi:[10.1103/PhysRevLett.11.146](https://doi.org/10.1103/PhysRevLett.11.146) (1963).
34. Jiang, A. Q., Lee, H. J., Hwang, C. S. & Scott, J. F. Sub-picosecond processes of ferroelectric domain switching from field and temperature experiments. *Advanced Functional Materials* **22**, 192–199, doi:[10.1002/adfm.201101521](https://doi.org/10.1002/adfm.201101521) (2012).
35. Mukhortov, V. M., Golovko, Y. I., Tolmachev, G. N. & Klevtsov, A. N. The synthesis mechanism of complex oxide films formed in dense RF-plasma by reactive sputtering of stoichiometric targets. *Ferroelectrics* **247**, 75–83, doi:[10.1080/000150190008214943](https://doi.org/10.1080/000150190008214943) (2000).
36. Yuzyuk, Y. I. *et al.* Influence of the growth mechanism and thermoelastic stresses on the lattice dynamics of heteroepitaxial films of barium strontium titanate. *Physics of the Solid State* **49**, 1759–1765, doi:[10.1134/S1063783407090247](https://doi.org/10.1134/S1063783407090247) (2007).
37. Anokhin, A. S., Razumnaya, A. G., Yuzyuk, Y. I., Golovko, Y. I. & Mukhortov, V. M. Phase transitions in barium-strontium titanate films on MgO substrates with various orientations. *Physics of the Solid State* **58**, 2027–2034, doi:[10.1134/S1063783416100048](https://doi.org/10.1134/S1063783416100048) (2016).
38. Padilla, J., Zhong, W. & Vanderbilt, D. First-principles investigation of 180° domain walls in BaTiO₃. *Physical Review B* **53**, R5969–R5973, doi:[10.1103/PhysRevB.53.R5969](https://doi.org/10.1103/PhysRevB.53.R5969) (1996).
39. Vicario, C. *et al.* High efficiency THz generation in DSTMS, DAST and OH1 pumped by Cr:forsterite laser. *Optics Express* **23**, 4573–4580, doi:[10.1364/OE.23.004573](https://doi.org/10.1364/OE.23.004573) (2015).

Acknowledgements

The work is supported by Russian Science Foundation (16-12-10520). The experiments were performed at the Joint Institute of High Temperature of the Russian Academy of Science in the Center “Femtosecond Laser Complex” with additional equipment provided by the Scientific–Research Center “UNO Electronics” of Moscow Technical University. The authors thank A. B. Granovskiy who helped to initiate the collaboration.

Author Contributions

A.V.K. together with M.B.A. conceived the project. K.A.G., N.A.I., A.V.O. and O.V.C. designed experimental set-up and carried out experiments. K.A.G. automated experimental set-up and prepared the figures. V.M.M. prepared the samples and performed electro-physical measurements. E.D.M. and N.E.S. performed data analysis and developed phenomenological description. E.D.M. and N.E.S. wrote the paper with contributions from A.V.K. and M.B.A. All authors discussed the results and commented on the manuscript.

Additional Information

Supplementary information accompanies this paper at doi:[10.1038/s41598-017-00704-9](https://doi.org/10.1038/s41598-017-00704-9)

Competing Interests: The authors declare that they have no competing interests.

Publisher's note: Springer Nature remains neutral with regard to jurisdictional claims in published maps and institutional affiliations.



Open Access This article is licensed under a Creative Commons Attribution 4.0 International License, which permits use, sharing, adaptation, distribution and reproduction in any medium or format, as long as you give appropriate credit to the original author(s) and the source, provide a link to the Creative Commons license, and indicate if changes were made. The images or other third party material in this article are included in the article's Creative Commons license, unless indicated otherwise in a credit line to the material. If material is not included in the article's Creative Commons license and your intended use is not permitted by statutory regulation or exceeds the permitted use, you will need to obtain permission directly from the copyright holder. To view a copy of this license, visit <http://creativecommons.org/licenses/by/4.0/>.

© The Author(s) 2017